Chapter 2
Wave Propagation in Periodic Structures

Wave propagation in periodic structures is closely related to propagation of waves in continuous media. Thus, dispersion parameters such as wavenumber and wave impedance or permeability and permittivity, can be used to describe the propagation of waves in one-dimensional periodic structures like loaded or artificial transmission lines and waveguides, and in two- and three-dimensional structures like artificial lenses, transmit arrays and meta surfaces. In this chapter, the connection between transmission line theory and effective material parameters, that can be used to describe the propagation of waves in periodic lattices, is investigated. Furthermore, based on a general form of a transmission line model and effective material parameters, a physical limitation for dispersion characteristics and corresponding equivalent circuit are derived. Finally, the effect of discretization and finite unit cell size in periodic structures on effective material parameters is considered.

2.1 Material Parameters of Distributed Periodic Structures

The propagation of a wave in a charge free material can be described by Maxwell's equations which in the frequency domain are [1]

$$\int_{\partial A} \mathbf{E}(\mathbf{r},\omega)\mathrm{d}\mathbf{s} = -\int_{A} j\omega\mathbf{B}(\mathbf{r},\omega)\mathrm{d}\mathbf{A} \Leftrightarrow \mathrm{rot}\,\mathbf{E}(\mathbf{r},\omega) = -j\omega\mathbf{B}(\mathbf{r},\omega), \tag{2.1}$$

$$\int_{\partial A} \mathbf{H}(\mathbf{r},\omega)\mathrm{d}\mathbf{s} = \int_{A} j\omega\mathbf{D}(\mathbf{r},\omega)\mathrm{d}\mathbf{A} \Leftrightarrow \mathrm{rot}\,\mathbf{H}(\mathbf{r},\omega) = j\omega\mathbf{D}(\mathbf{r},\omega), \tag{2.2}$$

$$\int_{\partial V} \mathbf{D}(\mathbf{r},\omega)\mathrm{d}\mathbf{A} = 0 \Leftrightarrow \mathrm{div}\,\mathbf{D}(\mathbf{r},\omega) = 0, \tag{2.3}$$

$$\int_{\partial V} \mathbf{B}(\mathbf{r},\omega)\mathrm{d}\mathbf{A} = 0 \Leftrightarrow \mathrm{div}\,\mathbf{B}(\mathbf{r},\omega) = 0 \tag{2.4}$$

© Springer International Publishing Switzerland 2016

M. Maasch, *Tunable Microwave Metamaterial Structures*, Springer Theses,
DOI 10.1007/978-3-319-28179-7_2

with the material equations of a linear material

$$\mathbf{B}(\omega) = \mu_0 \left[\mathbf{M}(\omega) + \mathbf{H}(\omega)\right] = \mu_0 \left[\bar{\bar{\chi}}_m(\omega) + 1\right] \mathbf{H}(\omega) = \bar{\bar{\mu}}(\omega)\mathbf{H}(\omega), \tag{2.5}$$

$$\mathbf{D}(\omega) = \varepsilon_0 \mathbf{E}(\omega) + \mathbf{P}(\omega) = \varepsilon_0 \left[\bar{\bar{\chi}}_e(\omega) + 1\right] \mathbf{E}(\omega) = \bar{\bar{\varepsilon}}(\omega)\mathbf{E}(\omega). \tag{2.6}$$

Under the condition of an isotropic and homogeneous material, the material tensor $\bar{\bar{\mu}}(\mathbf{r}, \omega)$ and $\bar{\bar{\varepsilon}}(\mathbf{r}, \omega)$ reduce to scalar values and (2.1)–(2.4) can be combined to the Helmholtz equation

$$\begin{Bmatrix} \Delta\mathbf{E}(\mathbf{r}, \omega) \\ \Delta\mathbf{H}(\mathbf{r}, \omega) \end{Bmatrix} - k^2(\omega) \begin{Bmatrix} \mathbf{E}(\mathbf{r}, \omega) \\ \mathbf{H}(\mathbf{r}, \omega) \end{Bmatrix} = 0 \tag{2.7}$$

describing propagation in materials with the complex material properties μ and ε and the complex wavenumber

$$k(\omega) = \pm\omega\sqrt{\mu(\omega)\varepsilon(\omega)}. \tag{2.8}$$

The electric and magnetic field are related by the wave impedance Z_w so that

$$\mathbf{H}(\mathbf{r}, \omega) = \frac{1}{Z_w(\omega)} \cdot \frac{k}{|k|} \cdot \frac{\mathbf{S}}{|\mathbf{S}|} \times \mathbf{E}(\mathbf{r}, \omega) \tag{2.9}$$

with $\mathbf{S}/|\mathbf{S}|$ being the unit vector pointing in the direction of the energy flux of the wave. Hence, the wave impedance becomes

$$Z_w(\omega) = \pm\sqrt{\frac{\mu(\omega)}{\varepsilon(\omega)}}. \tag{2.10}$$

Similarly, the propagation of waves on a transmission line in z-direction is determined by [2]

$$\frac{\partial}{\partial z} \begin{Bmatrix} V(z, \omega) \\ I(z, \omega) \end{Bmatrix} - Z'_{\mathrm{se}}(\omega) Y'_{\mathrm{sh}}(\omega) \begin{Bmatrix} V(z, \omega) \\ I(z, \omega) \end{Bmatrix} = 0 \tag{2.11}$$

where the per unit length impedance and admittance Z'_{se} and Y'_{sh} are defined as in the equivalent circuit of an infinitesimal short transmission line section in Fig. 2.1. The propagation constant

$$\gamma = \alpha + j\beta = \pm\sqrt{Z'_{\mathrm{se}}(\omega) Y'_{\mathrm{sh}}(\omega)} \tag{2.12}$$

and the characteristic impedance

$$Z_c = \pm\sqrt{\frac{Z'_{\mathrm{se}}(\omega)}{Y'_{\mathrm{sh}}(\omega)}}. \tag{2.13}$$

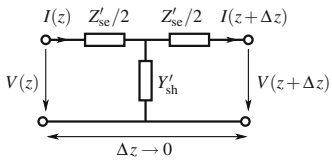


Fig. 2.1 Infinitesimal short transmission line section

are used to describe the wave propagation on transmission lines.

Due to the equivalence between the wave equations and the impedance definition of the plane wave propagation and the propagation on the transmission line it can be defined

$$Z'_{\mathrm{se}}(\omega) = \lim_{\Delta z \to 0} \frac{Z_{\mathrm{se}}(\omega)}{\Delta z} = j\omega\mu_{\mathrm{eff}}(\omega), \tag{2.14}$$

$$Y'_{\mathrm{sh}}(\omega) = \lim_{\Delta z \to 0} \frac{Y_{\mathrm{sh}}(\omega)}{\Delta z} = j\omega\varepsilon_{\mathrm{eff}}(\omega), \tag{2.15}$$

i.e. the material parameters μ, ε and transmission line elements Z'_{se}, Y'_{sh} are mathematically equivalent [3, 4]. Since the resulting material parameters are not necessarily the parameters of an existing material, but describe the response of a periodic structure to the propagating electric and magnetic field of an arbitrary wave, they are denoted as effective material parameters μ_{eff} and $\varepsilon_{\mathrm{eff}}$.

Propagation of a plane wave in a material can be described by the transmission line equivalent circuit in Fig. 2.1. On the other hand, wave propagation on a transmission line can be described by a wave propagating in an effective material with μ_{eff} and $\varepsilon_{\mathrm{eff}}$. Hence, by adjusting the series impedance Z'_{se} and the shunt admittance Y'_{sh}, the frequency characteristic of the magnetic and electric response can be designed independently of each other for the case of a guided wave on a transmission line as well as for propagation of plane waves.

2.2 Dispersion Functions and Transmission Line Model

The Lorentz model, a damped mechanical oscillator model, represents an accurate description of lossy dielectric materials with resonant or relaxation effects, plasmas, or lossy metals and semiconductors with free charges. This classical quantum-mechanical dispersion model is based on the motion of electrons with the charge e and the mass m_e [1]

$$\varepsilon(\omega) = \varepsilon_0 \left(1 - \frac{N_m e^2}{\varepsilon_0 m_e} \sum_i \frac{A_i}{\omega^2 - \omega_{0\varepsilon i}^2 - j\omega\delta_{\varepsilon i}} \right), \text{ with } \sum_i A_i = N_e \tag{2.16}$$

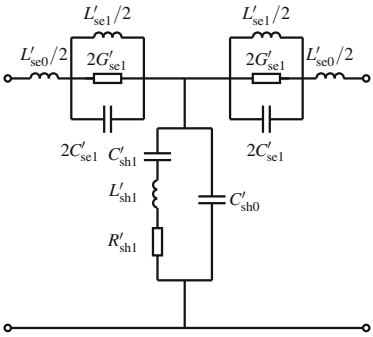


Fig. 2.2 Transmission line model of a Lorentz–Lorentz material

where N_m is the number of molecules per unit volume with N_e electrons per molecule, $\omega_{0\varepsilon i}$ is the resonance frequency, and $\delta_{\varepsilon i}$ the collision frequency or damping factor.

Setting $\omega_{0\varepsilon} = 0$ yields the Drude dispersion, e.g. of metals or plasmas with free electric charges [5]. On the contrary, the Debye dispersion where the collision frequency is in the range of the resonance frequency $\delta_\varepsilon \approx \omega_{0\varepsilon}$ describes relaxation effects, e.g. in dielectric or liquid materials [1]. The summation takes into account that a material can exhibit different resonance and relaxation effects based on different charges and their dipole moment. A material dispersion represented by the Lorentz equation is always causal since it is derived from a mechanical model that is per se causal [6].

With (2.14) and (2.15) it is possible to translate the Lorentz dispersion relation (2.16) into a transmission line model as in Fig. 2.1. For a single resonance of the permeability and permittivity, Fig. 2.2 shows a possible configuration of a transmission line model that yields a Lorentz dispersion for the effective permeability and permittivity. With (2.14) and (2.15), the effective material parameters become

$$\mu_{\text{eff}}(\omega) = \mu_\infty \frac{\omega^2 - \omega_{t\mu}^2 - j\omega\delta_\mu}{\omega^2 - \omega_{0\mu}^2 - j\omega\delta_\mu}, \tag{2.17}$$

$$\varepsilon_{\text{eff}}(\omega) = \varepsilon_\infty \frac{\omega^2 - \omega_{t\varepsilon}^2 - j\omega\delta_\varepsilon}{\omega^2 - \omega_{0\varepsilon}^2 - j\omega\delta_\varepsilon}, \tag{2.18}$$

which is a rearranged form of (2.16) with a pole and a zero in the complex omega plane at

$$\omega_{\text{pole}} = j\frac{\delta}{2} \pm \sqrt{\omega_0^2 - \frac{\delta^2}{4}} \tag{2.19}$$

and

$$\omega_{\text{zero}} = j\frac{\delta}{2} \pm \sqrt{\omega_t^2 - \frac{\delta^2}{4}}. \tag{2.20}$$

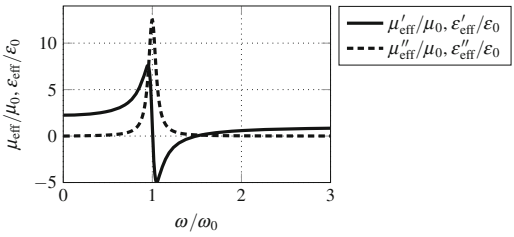


Fig. 2.3 Effective material parameters of a Lorentz–Lorentz material

The resonance frequency ω_0, the transition frequency ω_t, and the damping factor δ are determined by the element values:

$$\omega_{0\mu}^2 = \frac{1}{L'_{\text{se1}} C'_{\text{se1}}},\ \omega_{t\mu}^2 = \omega_{0\mu}^2 + \frac{1}{L'_{\text{se0}} C'_{\text{se1}}},\ \delta_\mu = \frac{G_{\text{se1}}}{C_{\text{se1}}},\ \mu_\infty = L'_{\text{se0}}, \tag{2.21}$$

$$\omega_{0\varepsilon}^2 = \frac{1}{L'_{\text{sh1}} C'_{\text{sh1}}},\ \omega_{t\varepsilon}^2 = \omega_{0\varepsilon}^2 + \frac{1}{L'_{\text{sh1}} C'_{\text{sh0}}},\ \delta_\varepsilon = \frac{R_{\text{sh1}}}{L_{\text{sh1}}},\ \varepsilon_\infty = C'_{\text{sh0}}. \tag{2.22}$$

Here, losses are assigned to the series capacitance C'_{se} and the shunt inductance L'_{sh}. However, losses in form of a series or parallel resistance can be added to each reactive element in the model which has an impact on the Lorentz parameters but not on the general dispersion equation.

Figure 2.3 shows the resulting complex effective material parameters for $\omega_t = 1.5\omega_0$ and $\delta = 0.1\omega_0$. At the resonance frequency ω_0, due to the pole, the real part becomes very large with a change of the sign so that between the resonance and the transition frequency ω_t, the real part is negative. Furthermore, the imaginary part, i.e. the loss, has its maximum at the resonance frequency and stays significant in the negative region above the resonance frequency.

In the quantum-mechanical model described by (2.16), charges that are bound in the material, e.g. in a lattice, yield a resonance effect as in the Lorentz dispersion. If these charges are not bound but can move freely (only limited by losses, e.g. by collisions), the resonance frequency shifts to zero yielding the Drude dispersion model with

$$\mu_{\text{eff}}(\omega) = \mu_\infty \frac{\omega^2 - \omega_{\text{p}\mu}^2 - j\omega\delta_\mu}{\omega^2 - j\omega\delta_\mu}, \tag{2.23}$$

$$\varepsilon_{\text{eff}}(\omega) = \varepsilon_\infty \frac{\omega^2 - \omega_{\text{p}\varepsilon}^2 - j\omega\delta_\varepsilon}{\omega^2 - j\omega\delta_\varepsilon}. \tag{2.24}$$

It exhibits complex poles and zeros at

$$\omega_{\text{pole1}} = 0,\ \omega_{\text{pole2}} = j\delta \tag{2.25}$$

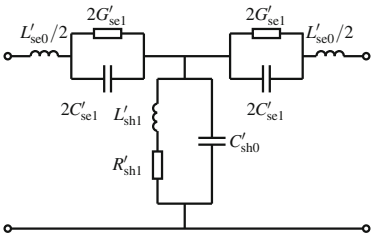


Fig. 2.4 Transmission line model of a Drude–Drude material

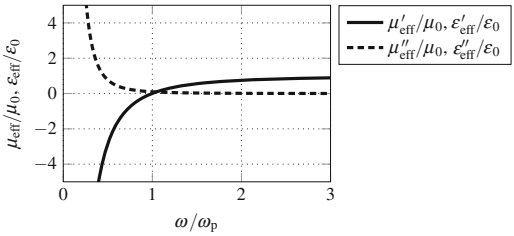


Fig. 2.5 Effective material parameters of a Drude–Drude material

and

$$\omega_{zero} = j\frac{\delta}{2} \pm \sqrt{\omega_p^2 - \frac{\delta^2}{4}}. \tag{2.26}$$

These dispersion properties can be translated into the transmission line model in Fig. 2.4 so that

$$\omega_{p\mu}^2 = \frac{1}{L'_{se0}C'_{se1}},\ \delta_\mu = \frac{G_{se1}}{C_{se1}},\ \mu_\infty = L'_{se0}, \tag{2.27}$$

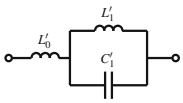
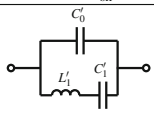
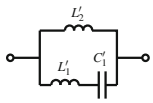
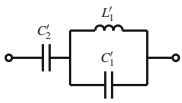
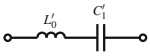
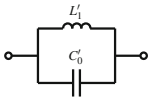
$$\omega_{p\varepsilon}^2 = \frac{1}{L'_{sh1}C'_{sh0}},\ \delta_\varepsilon = \frac{R_{sh1}}{L_{sh1}},\ \varepsilon_\infty = C'_{sh0}. \tag{2.28}$$

For $\delta = 0.1\omega_p$, the effective material parameters are shown in Fig. 2.5. For frequencies below the plasma frequency ω_p, the real part is negative and continuously increasing while above ω_p it is positive. Compared to the Lorentz dispersion, the region of a negative real part is much wider due to the shift of the resonance frequency to zero. Furthermore, the loss is increasing for lower frequencies and has its maximum at zero.

The translation of the dispersion equation (2.16) into a transmission line model is not unambiguous if it exhibits one or more non-zero resonances or poles, i.e. the translation of (2.17) and (2.18) yields more than a single solution. Table 2.1 shows the series impedance Z'_{se} and shunt admittance Y'_{sh} for the lossless case[1] $\delta_\mu = \delta_\varepsilon = 0$ to model the Lorentz and Drude dispersion with a transmission line model (2.16). It

[1] Losses can be taken into account by adding a resistance to each necessary reactive element, yielding $\delta > 0$.

Table 2.1 Series and shunt branch impedances (without losses) which create a Drude and Lorentz dispersion

Dispersion model	series branch $Z'_{se} \rightarrow \mu_{eff}$	shunt branch $Y'_{sh} \rightarrow \varepsilon_{eff}$
Lorentz: $\mu_{eff}, \varepsilon_{eff} = A\frac{\omega^2-\omega_t^2}{\omega^2-\omega_0^2}$	 $A = L'_0$ $\omega_0^2 = \frac{1}{L'_1 C'_1}$ $\omega_t^2 = \omega_0^2 + \frac{1}{L'_0 C'_1}$	 $A = C'_0$ $\omega_0^2 = \frac{1}{L'_1 C'_1}$ $\omega_t^2 = \omega_0^2 + \frac{1}{L'_1 C'_0}$
	 $A = \frac{L'_1 L'_2}{L'_1 + L'_2}$ $\omega_0^2 = \frac{1}{(L'_1+L'_2)C'_1}$ $\omega_p^2 = \frac{1}{L'_1 C'_1}$	 $A = \frac{C'_1 C'_2}{C'_1 + C'_2}$ $\omega_0^2 = \frac{1}{L'_1(C'_1+C'_2)}$ $\omega_p^2 = \frac{1}{L'_1 C'_1}$
Drude: $\mu_{eff}, \varepsilon_{eff} = A\frac{\omega^2-\omega_p^2}{\omega^2}$	 $A = L'_0$ $\omega_0^2 = 0$ $\omega_p^2 = \frac{1}{L'_0 C'_1}$	 $A = C'_0$ $\omega_0^2 = 0$ $\omega_p^2 = \frac{1}{L'_1 C'_0}$

can be seen that the Lorentz dispersion yields two solutions for each, the series and shunt branch, while the solution for the Drude dispersion is unambiguous.

With the effective material parameters, the wavenumber (2.8) can be determined. The sign of the square root determines, whether the phase is propagating in forward or backward direction with parallel or anti-parallel[2] wave vector $\mathbf{k}$ and Poynting vector $\mathbf{S}$, respectively, so that

$$\frac{k}{|k|} \cdot \frac{\mathbf{S}}{|\mathbf{S}|} = \pm 1. \tag{2.29}$$

A positive product $\mu'_{eff}\varepsilon'_{eff}$ yields forward propagation whereas for backward propagation, i.e. for a negative product, (2.29) becomes negative [8]. Hence, with the wavenumber (2.8), the phase velocity

$$v_p = \frac{\omega}{\mathrm{Re}\{k(\omega)\}} \tag{2.30}$$

can take positive and negative values. However, for small losses

[2] In a two- or three-dimensonal anisotropic material, the angle between the Poynting vector and wave vector can have arbitrary values [7].

$$\frac{\mu''_{\text{eff}}}{\mu'_{\text{eff}}}, \frac{\varepsilon''_{\text{eff}}}{\varepsilon'_{\text{eff}}} \ll 1 \tag{2.31}$$

the group velocity

$$v_g = \frac{\partial \omega}{\partial \text{Re}\{k\}} \tag{2.32}$$

corresponds to the energy velocity v_e which always has to be positive.

The transmission line model and (2.14) and (2.15) indicate that the effective material parameters can be set independently of each other. Hence, arbitrary configurations of the series and shunt branch are possible to create a required dispersion characteristic. In Sect. 2.4 it will be shown that this separation of the magnetic and electric response is only possible for an infinitesimal short transmission line section.

2.3 Causality and Its Consequences on Dispersion

In the previous section, the quantum-mechanical Lorentz model, and hence, a physically realizable model, was used to find the transmission line model of materials and metamaterials with dispersive characteristics. In this section, realizability of a transmission line model is investigated directly by taking the concept of stability and causality into account.

The effective material parameters of an arbitrary medium can be described by its magnetic and electric susceptibility $\chi_m(\omega)$ and $\chi_e(\omega)$ so that

$$\mu_{\text{eff}}(\omega) = \mu'_{\text{eff}} - j\mu''_{\text{eff}} = -j\frac{Z'_{\text{se}}(\omega)}{\omega} = a_m \mu_0 \left[\chi_m(\omega) + 1\right], \tag{2.33}$$

$$\varepsilon_{\text{eff}}(\omega) = \varepsilon'_{\text{eff}} - j\varepsilon''_{\text{eff}} = -j\frac{Y'_{\text{sh}}(\omega)}{\omega} = a_e \varepsilon_0 \left[\chi_e(\omega) + 1\right], \tag{2.34}$$

where a_m and a_e account the field distribution of the propagating wave different from a plane wave, e.g. if the host medium is a microstrip transmission line or a hollow wave guide. For plane wave propagation in vacuum $a_m = a_e = 1$. The susceptibility describes the polarization and magnetization of a material, i.e. in time domain the response to an external electric or magnetic field [9]

$$\mathbf{M}(t) = \chi_m(t) * \mathbf{H}(t) = \left[\chi'_m(t) - j\chi''_m(t)\right] * \mathbf{H}(t), \tag{2.35}$$

$$\mathbf{P}(t) = \varepsilon_0 \chi_e(t) * \mathbf{E}(t) = \left[\chi'_e(t) - j\chi''_e(t)\right] * \mathbf{E}(t). \tag{2.36}$$

Since investigation of causality and dispersion is equivalent for the magnetic and electric susceptibility, the general susceptibility $\chi(t)$ with its Fourier transform

$$\chi(\omega) = \mathcal{F}\{\chi(t)\} = \frac{1}{2\pi}\int_{-\infty}^{\infty} \chi(t) e^{-j\omega t} \mathrm{d}t \tag{2.37}$$

is used for both quantities.

Without an external field, the considered material does not exhibit a polarization or magnetization. Hence, the time response $\chi(t)$ has to vanish for negative times which is a general condition for a causal system [10]. According to Titchmarsh's theorem [11, 12], if the square integrability

$$\int_{-\infty}^{\infty} |\chi(\omega)|^2 \mathrm{d}\omega \leq C < \infty \tag{2.38}$$

is fulfilled, i.e. the total energy within the system is bounded and cannot be infinitely large [10], the following statements are equivalent, and if one of the conditions is met, all others are automatically fulfilled:

(i) the time response of the susceptibility vanishes for negative times:

$$\chi(t) = 0 \quad \forall \quad t < 0, \tag{2.39}$$

(ii) the real and imaginary part of the frequency response are connected by the Hilbert transform

$$\chi(\omega) = -j\mathcal{H}\{\chi(\omega)\} = -\frac{j}{\pi} \fint_{-\infty}^{\infty} \frac{\chi(\Omega)}{\omega - \Omega} \mathrm{d}\Omega, \tag{2.40}$$

(iii) the frequency response $\chi(\omega)$ is analytic in the lower half of the complex ω plane.

All three conditions distinguish a causal time response $\chi(t)$ under the condition of bounded energy (2.38). If $\chi(t)$ is a purely real time response (which is the case for a physical realizable time response), it can be split up into a real even and real odd part which yields together with (i) and the symmetry of the Fourier transform [9, 13]

$$\chi(-\omega) = \chi^*(\omega). \tag{2.41}$$

Thus, for a causal response, the real part $\chi'(\omega)$ has to be an even function while the imaginary part $-\chi''(\omega)$ has to be an odd function over frequency. With that, the integration in (2.38) is symmetric and

$$\int_{-\infty}^{\infty} |\chi(\omega)|^2 \mathrm{d}\omega = 2\int_{0}^{\infty} |\chi(\omega)|^2 \mathrm{d}\omega \leq C < \infty. \tag{2.42}$$

To fulfill the bounded energy criterion (2.42) the susceptibility has to vanish in the high frequency limit so that

$$\lim_{\omega\to\infty}\chi(\omega)=0. \tag{2.43}$$

Hence, with (2.33) and (2.34) the effective material parameters have to follow

$$\mu_\infty=\lim_{\omega\to\infty}\mu_{\text{eff}}=\lim_{\omega\to\infty}\frac{Z'_{\text{se}}(\omega)}{j\omega}=a_m\mu_0:=L'_0, \tag{2.44}$$

$$\varepsilon_\infty=\lim_{\omega\to\infty}\varepsilon_{\text{eff}}=\lim_{\omega\to\infty}\frac{Y'_{\text{sh}}(\omega)}{j\omega}=a_e\varepsilon_0:=C'_0, \tag{2.45}$$

so that at high frequencies the wave propagation is determined only by the host medium with

$$L'_0=a_m\mu_0>0, \tag{2.46}$$

$$C'_0=a_e\varepsilon_0>0. \tag{2.47}$$

Consequently it is not possible to realize arbitrary unit cell configurations. Instead, the unit cell has to consist of at least a series inductance and shunt admittance which do not vanish in the high frequency limit.

Based on that, the series and shunt branch of a general unit cell can be described as shown in Fig. 2.6 by the distributed complex impedance and admittance

$$Z'_{\text{se}}(\omega)=\cfrac{1}{Y'_{\text{se}M}+\cfrac{1}{Z'_{\text{se}M}+\cdots\cfrac{1}{Y'_{\text{se}2}+\cfrac{1}{Z'_{\text{se}2}+\cfrac{1}{Y'_{\text{se}1}+\cfrac{1}{Z'_{\text{se}1}+j\omega L'_0}}}}}}, \tag{2.48}$$

$$Y'_{\text{sh}}(\omega)=\cfrac{1}{Z'_{\text{sh}N}+\cfrac{1}{Y'_{\text{sh}N}+\cdots\cfrac{1}{Z'_{\text{sh}2}+\cfrac{1}{Y'_{\text{sh}2}+\cfrac{1}{Z'_{\text{sh}1}+\cfrac{1}{Y'_{\text{sh}1}+j\omega C'_0}}}}}}, \tag{2.49}$$

with the non-zero elements L'_0 and C'_0. Furthermore, in the high frequency limit, the impact of all elements except L'_0 and C'_0 has to vanish, i.e.

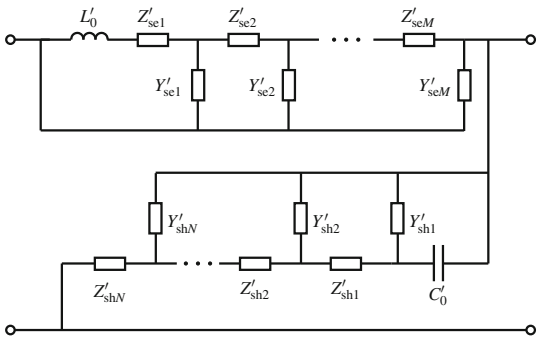


Fig. 2.6 Series and shunt branch impedance and admittance including the minimal required elements L'_0 and C'_0 in the series and shunt branch

$$\lim_{\omega\to\infty} \frac{Z'_n(\omega)}{j\omega} = \lim_{\omega\to\infty} \frac{Y'_n(\omega)}{j\omega} = 0. \tag{2.50}$$

Z'_n and Y'_n are not restricted to purely reactive elements but can also contain resistive elements as long as the high frequency condition (2.44) and (2.45) is fulfilled.

Although other topologies for Z'_{se} and Y'_{sh} are possible, the high frequency condition (2.44) and (2.45), which ensures the square integrability (2.42), has to hold for any topology.

2.3.1 Application to Different Unit Cell Configurations

Different unit cell configurations exist to realize a desired dispersion characteristic. If investigated over frequency, not all of them follow (2.44) and (2.45). Thus, not all unit cell configurations fulfill the bounded energy criterion (2.38) and are physically realizable. By using condition (2.43) it is possible to find the physical equivalent circuit of arbitrary unit cell topologies or to test a given unit cell configuration for its realizability and to investigate its high frequency response.

As an example, below, different common unit cell configurations are investigated in terms of causality and their physical realizability.

Microstrip Transmission Line

A microstrip transmission line on a Rogers Duroid 5880 substrate with a copper metallization with a thickness of 17 µm and the dimensions as shown in Fig. 2.7a yields a characteristic impedance $Z_c = (50.16 - j84.66 \times 10^{-9})\,\Omega$ and a phase constant $\gamma = (0.1456 + j290.8)\,\mathrm{m}^{-1}$ at a frequency of 10 GHz.

With (2.12) and (2.13) the distributed unit cell elements become

$$Z'_{\mathrm{se}} = \gamma \cdot Z_c = 7.304\,\Omega/\mathrm{m} + j\omega 0.184\mu_0, \tag{2.51}$$

$$Y'_{\mathrm{sh}} = \gamma / Z_c = 2.903 \times 10^{-3}\mathrm{S/m} + j\omega 10.42\varepsilon_0. \tag{2.52}$$

This corresponds to the transmission line equivalent circuit in Fig. 2.7b with a constant per unit length resistance and inductance in the series branch and a constant

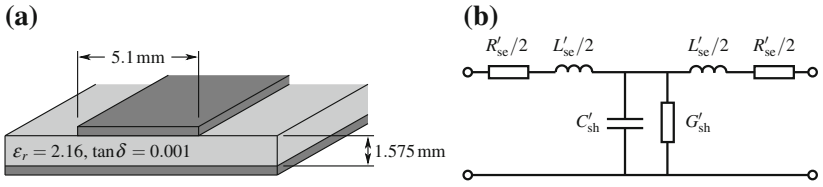


Fig. 2.7 Investigated microstrip transmission line: **a** Cross-section view, **b** transmission line equivalent circuit

per unit length conductance and capacitance in the shunt branch as expected from transmission line theory. Hence, (2.44) and (2.45) yield the high frequency limit

$$\mu_\infty = \lim_{\omega\to\infty}\left(\frac{R'_{\mathrm{se}}}{j\omega} + L'_{\mathrm{se}}\right) = L'_0 = a_m\mu_0 = 0.184\mu_0, \tag{2.53}$$

$$\varepsilon_\infty = \lim_{\omega\to\infty}\left(\frac{G'_{\mathrm{sh}}}{j\omega} + C'_{\mathrm{sh}}\right) = C'_0 = a_e\varepsilon_0 = 10.42\varepsilon_0, \tag{2.54}$$

i.e. the bounded energy criterion (2.42) is fulfilled and in the high frequency limit the dispersion is determined by the series inductance and shunt capacitance. Thus, the unit cell is realizable in its current form.

Left-Handed Unit Cell

A left-handed unit cell as depicted in Fig. 2.8 consists of a series capacitance and a shunt inductance [14]. Adding resistive losses yields the series impedance and shunt admittance

$$Z'_{\mathrm{se,LH}}(\omega) = R'_{\mathrm{se}} + \frac{1}{j\omega C'_{\mathrm{se}}}, \tag{2.55}$$

$$Y'_{\mathrm{sh,LH}}(\omega) = G'_{\mathrm{se}} + \frac{1}{j\omega L'_{\mathrm{sh}}}. \tag{2.56}$$

In the high frequency limit, the complex effective material parameters become

$$\mu_\infty = \lim_{\omega\to\infty}\frac{Z'_{\mathrm{se,LH}}(\omega)}{j\omega} = \varepsilon_\infty = \lim_{\omega\to\infty}\frac{Y'_{\mathrm{sh,LH}}(\omega)}{j\omega} = 0 \tag{2.57}$$

as shown for the effective permeability in Fig. 2.9. L'_0 and C'_0 in Eqs. (2.48) and (2.49) are zero and hence, the magnetic and electric susceptibility do not vanish for large frequencies. Thus, the square integrability (2.42) and the conditions (i)–(iii) are not fulfilled.

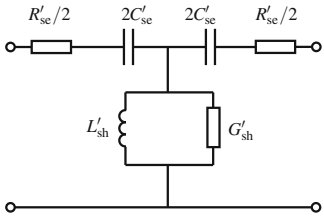


Fig. 2.8 Unit cell configuration of a lossy left-handed transmission line

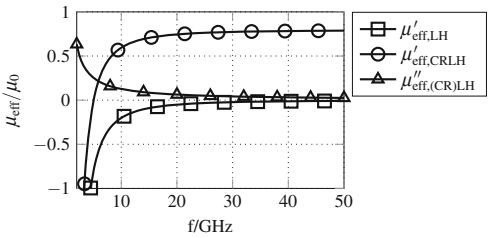


Fig. 2.9 Comparison of the effective permeability of a distributed purely LH and CRLH transmission line ($R'_{\text{se}} = 10\,\text{k}\Omega/\text{m}$, $L'_0 = 1\,\mu\text{H/m}$, $C'_{\text{se}} = 1\,\text{fF}\cdot\text{m}$)

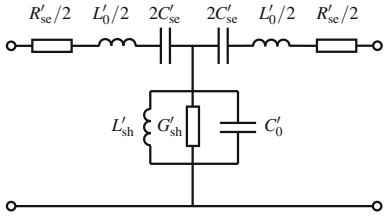


Fig. 2.10 Unit cell configuration of a lossy composite left-handed transmission line

Adding a non-zero L'_0 and C'_0 as in (2.48) and (2.49) yields the composite right/left-handed (CRLH) unit cell [15] as depicted in Fig. 2.10 with the Drude dispersion (2.23) and (2.24) created by

$$Z'_{\text{se,CRLH}} = R'_{\text{se}} + j\left(\omega L'_0 - \frac{1}{\omega C'_{\text{se}}}\right), \tag{2.58}$$

$$Y'_{\text{sh,CRLH}} = G'_{\text{se}} + j\left(\omega C'_0 - \frac{1}{\omega L'_{\text{sh}}}\right). \tag{2.59}$$

The unit cell consists of a series resonator in the series branch and a parallel resonator in the shunt branch with the magnetic and electric plasma frequency

$$\omega_{\text{p}\mu} = \frac{1}{\sqrt{L'_0 C'_{\text{se}}}},\ \omega_{\text{p}\varepsilon} = \frac{1}{\sqrt{L'_{\text{sh}} C'_0}}. \tag{2.60}$$

Thus, a non-zero value of L'_0 and C'_0 ensures a finite magnetic and electric plasma frequency, respectively. For the high frequency limit that yields

$$\mu_\infty = \lim_{\omega\to\infty}\left(\frac{R'_{\text{se}}}{j\omega} + L'_0 - \frac{1}{\omega^2 C'_{\text{se}}}\right) = L'_0 \tag{2.61}$$

and

$$\varepsilon_\infty = \lim_{\omega\to\infty}\left(\frac{G'_{\text{sh}}}{j\omega} + C'_0 - \frac{1}{\omega^2 L'_{\text{sh}}}\right) = C'_0 \tag{2.62}$$

which can be seen for the effective permeability in Fig. 2.9. The effective permeability in the high frequency limit does not vanish but reaches a constant value. The same holds for the frequency response of the effective permittivity.

A more practical explanation takes the physical implementation and realizability of a unit cell into consideration. The elements C'_{se} and L'_{sh} have to be embedded in a host medium, e.g. a microstrip line, which can be described by a per unit length series inductance and shunt capacitance. Hence, the series inductance L'_0 and shunt capacitance C'_0 can be considered as parasitic effects created by the host medium.

Dual Composite Right/Left-Handed Unit Cell

The series impedance and shunt admittance of a dual composite right/left-Handed (D-CRLH) unit cell in Fig. 2.11, consisting of a parallel resonator in the series branch and a series resonator in the shunt branch [16], are

$$Z'_{\mathrm{se,DCRLH}}(\omega) = \frac{1}{G'_{\mathrm{se}} + j\left(\omega C'_{\mathrm{se}} - \frac{1}{\omega L'_{\mathrm{se}}}\right)}, \tag{2.63}$$

$$Y'_{\mathrm{sh,DCRLH}}(\omega) = \frac{1}{R'_{\mathrm{sh}} + j\left(\omega L'_{\mathrm{sh}} - \frac{1}{\omega C'_{\mathrm{sh}}}\right)}. \tag{2.64}$$

The high frequency limit becomes

$$\mu_\infty = \lim_{\omega\to\infty} \frac{Z'_{\mathrm{se,DCRLH}}(\omega)}{j\omega} = \varepsilon_\infty = \lim_{\omega\to\infty} \frac{Y'_{\mathrm{sh,DCRLH}}(\omega)}{j\omega} = 0 \tag{2.65}$$

and the condition of square integrability (2.42) is not fulfilled.

The effective material parameters

$$\mu_{\mathrm{eff}} = -\frac{1}{C'_{\mathrm{se}}} \cdot \frac{1}{\omega^2 - \omega_{0\mu} - j\omega\delta_\mu}, \tag{2.66}$$

$$\varepsilon_{\mathrm{eff}} = -\frac{1}{L'_{\mathrm{sh}}} \cdot \frac{1}{\omega^2 - \omega_{0\varepsilon} - j\omega\delta_\varepsilon} \tag{2.67}$$

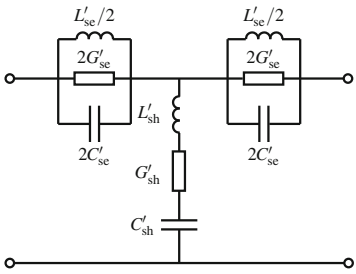


Fig. 2.11 Unit cell configuration of a lossy dual composite left-handed transmission line

reveal a Lorentz dispersion with the magnetic and electric resonance frequency

$$\omega_{0\mu} = \frac{1}{\sqrt{L'_{\mathrm{se}} C'_{\mathrm{se}}}}, \quad \omega_{0\varepsilon} = \frac{1}{\sqrt{L'_{\mathrm{sh}} C'_{\mathrm{sh}}}} \tag{2.68}$$

and the magnetic and electric damping factors

$$\delta_\mu = \frac{G'_{\mathrm{se}}}{C'_{\mathrm{se}}}, \quad \delta_\varepsilon = \frac{R'_{\mathrm{sh}}}{L'_{\mathrm{sh}}}. \tag{2.69}$$

However, a transition frequency, i.e. a zero in the dispersion equations where the sign of the real part changes from negative to positive, does not exist. Hence, above the resonance frequency, the real part of the effective material parameters is negative for all frequencies $\omega > \omega_0$.

Addition of the series inductance L'_0 in the series branch and the parallel capacitance C'_0 in the shunt branch yields the effective material parameters

$$\mu_{\mathrm{eff}} = L'_0 \left(1 - \frac{\omega_{\mathrm{t}\mu}^2 - \omega_{0\mu}^2}{\omega^2 - \omega_{0\mu}^2 - j\omega\delta_\mu} \right), \tag{2.70}$$

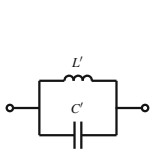
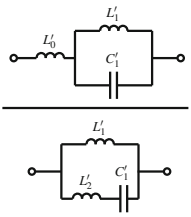
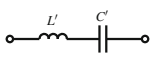
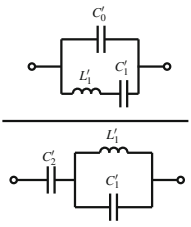
$$\varepsilon_{\mathrm{eff}} = C'_0 \left(1 - \frac{\omega_{\mathrm{t}\varepsilon}^2 - \omega_{0\varepsilon}^2}{\omega^2 - \omega_{0\varepsilon}^2 - j\omega\delta_\varepsilon} \right) \tag{2.71}$$

following the Lorentz dispersion (2.17) and (2.18). As for the CRLH unit cell, $L'_0 = \mu_\infty$ and $C'_0 = \varepsilon_\infty$ ensure the square integrability (2.42) as well as a finite magnetic and electric transition frequency

$$\omega_{\mathrm{t}\mu} = \sqrt{\omega_{0\mu}^2 + \frac{1}{L'_0 C'_{\mathrm{se}}}}, \quad \omega_{\mathrm{t}\varepsilon} = \sqrt{\omega_{0\varepsilon} + \frac{1}{C'_0 L'_{\mathrm{sh}}}}. \tag{2.72}$$

The general configuration in Fig. 2.6 indicates that for the D-CRLH unit cell, the addition of the inductance in the series branch and capacitance in the shunt branch can be done at different positions of the unit cell to enforce the square integrability. As shown in Table 2.2, an inductance L'_0 and capacity C'_0 can be added in series and parallel of the original series and shunt branch, respectively, which has been done in the previous investigation. Another possibility is the addition of L'_2 and C'_2, which also yields a correct Lorentz dispersion with a finite transition frequency and a positive high frequency limit (2.44) and (2.45). The corrected unit cell configurations correspond to the Lorentz- and Drude dispersion models derived before in Sect. 2.2. The number of possible positions is increased with the number of elements (M, N in (2.48) and (2.49)) in the unit cell. The resulting series impedance and shunt admittance are closely related to reactances and its negative reciprocals, respectively, in the form a Foster network [17]. The difference is that in the present topology, losses can be taken into account by the use of complex poles and zeros in the impedance and admittance function.

Table 2.2 D-CRLH unit cell elements with corrected series- and shunt impedance and admittance

	Original	Corrected
Series branch impedance Z'_{se}		
Shunt branch admittance Y'_{sh}		

2.3.2 *Kramers–Kronig Relation for Phase Reconstruction*

The Hilbert transform (2.40), also known as Kramers–Kronig relation [11, 12], relates the real and imaginary part of complex transfer functions of causal and stable systems. Here, these transfer functions are the magnetizability χ_m and polarizability χ_e of a continuous material or periodic structure.

The complex wavenumber k can be expressed by the material parameters so that

$$k^2(\omega) = k_0^2(\omega)\,[1 + \chi_m(\omega)]\,[1 + \chi_e(\omega)]\,, \tag{2.73}$$

where k_0 is the free space wavenumber

$$k_0(\omega) = \omega\sqrt{\mu_0\varepsilon_0}. \tag{2.74}$$

For a causal and stable material, Titchmarsh's theorem and hence, the Kramers–Kronig relation (2.40) has to be fulfilled for $\chi_m(\omega)$ and $\chi_e(\omega)$. Since the symmetry (2.41) of the real and imaginary parts after the multiplication of both susceptibilities is maintained, the square of the wavenumber in the form

$$\frac{k^2(\omega)}{k_0^2(\omega)} - 1 = \chi_m(\omega) + \chi_e(\omega) + \chi_m(\omega)\chi_e(\omega) \tag{2.75}$$

is a causal spectrum so that the Kramers–Kronig relation can be applied and

$$\frac{k^2(\omega)}{k_0^2(\omega)} = 1 - \frac{j}{\pi} \fint_{-\infty}^{\infty} \frac{k^2(\Omega)/k_0^2(\Omega)}{\omega - \Omega} \mathrm{d}\Omega. \tag{2.76}$$

The integral denotes the Cauchy principal value

$$\fint_a^b f(x)\mathrm{d}x = \lim_{\epsilon \to 0+} \left(\int_a^{c-\epsilon} f(x)\mathrm{d}x + \int_{c+\epsilon}^b f(x)\mathrm{d}x \right). \tag{2.77}$$

A detailed derivation taking into account the symmetry (2.41) can be found in Appendix A.1.

The Kramers–Kronig relation can be applied to the square of the wavenumber $k^2(\omega)$ or to the square of the refractive index [18]

$$n^2(\omega) = \frac{k^2(\omega)}{k_0^2(\omega)} \tag{2.78}$$

while an application directly to the wavenumber as in extraction methods [19, 20] is in general not possible since the causality of $k(\omega)$ is not necessarily maintained by the square root [18]. For small susceptibilities, however, it can be approximated

$$k(\omega) \approx k_0(\omega) \left(1 + \frac{\chi_m(\omega)}{2}\right) \left(1 + \frac{\chi_e(\omega)}{2}\right) \tag{2.79}$$

which has, concerning the susceptibilities, the form of (2.73) so that the Kramers–Kronig relation can be approximated and

$$\frac{k(\omega)}{k_0(\omega)} \approx 1 - \frac{j}{\pi} \fint_{-\infty}^{\infty} \frac{k(\Omega)/k_0(\Omega)}{\omega - \Omega} \mathrm{d}\Omega. \tag{2.80}$$

For the real part of the wavenumber this yields

$$\frac{\mathrm{Re}\{k(\omega)\}}{k_0(\omega)} \approx 1 + \frac{1}{\pi} \fint_{-\infty}^{\infty} \frac{\mathrm{Im}\{k(\Omega)\}/k_0(\Omega)}{\omega - \Omega} \mathrm{d}\Omega. \tag{2.81}$$

With that, the wavenumber, which in many extraction methods is ambiguous, can be determined from the losses, expressed by the non-ambiguous imaginary part $\mathrm{Im}\{k\}$. Due to the symmetry (2.41), integration only of the positive part of the spectrum is necessary

$$\frac{\mathrm{Re}\{k(\omega)\}}{k_0(\omega)} \approx 1 + \frac{2}{\pi} \fint_0^{\infty} \frac{\omega \mathrm{Im}\{k(\Omega)\}/k_0(\Omega)}{\omega^2 - \Omega^2} \mathrm{d}\Omega \tag{2.82}$$

which is used in phase reconstruction methods [19, 20] and later in extraction of effective material parameters in Sect. 4.1.

2.4 Effective Material Parameters of Discrete Periodic Structures

In passive, continuous media, Maxwell's equations (2.1)–(2.4) and the material relations (2.5) and (2.6) are defined for the same point $\mathbf{r}$ in space. $\mathbf{D}(t, \mathbf{r})$ is determined by $\mathbf{E}(t', \mathbf{r})$ and $\mathbf{B}(t, \mathbf{r})$ by $\mathbf{H}(t', \mathbf{r})$ in the same point with a temporal dispersion caused by the material. However, in a discretized, effective material, this is not fulfilled anymore since the response in the point $\mathbf{r}$ is determined by the field in the point $\mathbf{r}'$. The physical distance $\left|\mathbf{r} - \mathbf{r}'\right|$ between these two points causes a phase difference between $\mathbf{D}(t, \mathbf{r})$ and $\mathbf{E}(t', \mathbf{r}')$, and between $\mathbf{B}(t, \mathbf{r})$ and $\mathbf{H}(t', \mathbf{r}')$, respectively. Since this dispersion is caused by the spatial separation of the magnetic response and the electric response, it is called spatial dispersion [9].

The effect of spatial dispersion can be considered in the transmission line model. Up to this point it was assumed that the impedance and admittance to design a desired dispersion are distributed elements in an infinitesimal short unit cell, i.e. impedance and admittance can be defined over an infinitesimal short section. In a real implementation, such distributed elements cannot be realized since they cannot be arbitrarily scaled down in size but will always have a finite physical extent. Hence, lumped elements have to be used to approximate the distributed values

$$Z'_{\mathrm{se}}(\omega) = \lim_{\Delta z \to 0} \frac{Z_{\mathrm{se}}(\omega)}{\Delta z} \approx \frac{1}{\Delta z} Z_{\mathrm{se}}(\omega), \tag{2.83}$$

$$Y'_{\mathrm{sh}}(\omega) = \lim_{\Delta z \to 0} \frac{Y_{\mathrm{sh}}(\omega)}{\Delta z} \approx \frac{1}{\Delta z} Y_{\mathrm{sh}}(\omega). \tag{2.84}$$

Material parameters derived from field values at the interface of such discretized structures are non-local. Another explanation is based on the phase response of the unit cell. With increasing frequency, a periodic structure with distributed elements can provide an infinitely large phase shift since it consists of an infinite number of unit cells. If these distributed elements are replaced by lumped elements, the unit cell number in a certain physical length becomes finite and hence, the maximum phase shift is limited. Here, the impact of this discretization on effective material parameters, which has to be taken into account under certain conditions, is investigated.

The Bloch impedance, i.e. the characteristic impedance of periodic structures,

$$Z_B = \pm\sqrt{\frac{\mu_{\mathrm{eff}}}{\varepsilon_{\mathrm{eff}}}} \tag{2.85}$$

and the wavenumber

$$k = \pm\omega\sqrt{\mu_{\mathrm{eff}}\varepsilon_{\mathrm{eff}}} \tag{2.86}$$

can be used to describe the wave propagation in periodic, discrete structures equivalent to the propagation in homogenous materials [21]. Since for the discrete case

these parameters not only depend on the element values, but also on the unit cell configuration, different topologies are investigated.

Unit Cell in T-Configuration

Figure 2.12 shows an unsymmetric unit cell in T-configuration. The unit cell length p is finite and non-zero and using the chain parameters, the port voltages and currents of the n-th unit cell in an infinite array become

$$V[np] = V[(n+1)p](1 + Z_1Y_2) + I[(n+1)p](Z_1 + Z_2 + Z_1Y_2Z_3), \quad (2.87)$$

$$I[np] = V[(n+1)p]Y_2 + I[(n+1)p](1 + Y_2Z_3). \quad (2.88)$$

Due to the periodicity, the Floquet–Bloch theorem [21] with the periodic boundary condition

$$V[(n+1)p] = V[np]e^{-jk^{(\mathrm{T})}p}, \quad (2.89)$$

$$I[(n+1)p] = I[np]e^{-jk^{(\mathrm{T})}p} \quad (2.90)$$

yields

$$V[np] = V[np](1 + Z_1Y_2)e^{-jk^{(\mathrm{T})}p} + I[np](Z_1 + Z_2 + Z_1Y_2Z_3)e^{-jk^{(\mathrm{T})}p}, \quad (2.91)$$

$$I[np] = V[np]Y_2e^{-jk^{(\mathrm{T})}p} + I[np](1 + Y_2Z_3)e^{-jk^{(\mathrm{T})}p}. \quad (2.92)$$

The Bloch impedance of a periodic structure is defined as the ratio of the voltage and current at each unit cell interface and has to be independent of the position n of the infinite array:

$$Z_B[np] = \frac{V[np]}{I[np]} \overset{!}{=} Z_B[(n+1)p] = \frac{V[(n+1)p]}{I[(n+1)p]}. \quad (2.93)$$

That yields the two conditions

$$Z_B^{(\mathrm{T})} = \frac{Z_1 + Z_3 + Z_1Y_2Z_3}{e^{jk^{(\mathrm{T})}p} - (1 + Z_1Y_2)} \quad (2.94)$$

and

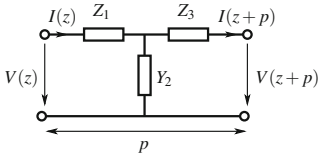


Fig. 2.12 Unsymmetric unit cell in T-configuration

$$Z_B^{(\mathrm{T})} = \frac{e^{jk^{(\mathrm{T})}p} - (1 + Y_2 Z_3)}{Y_2} \tag{2.95}$$

and thus,

$$Z_B^{(\mathrm{T})} = \frac{Z_1 - Z_3}{2} \pm \sqrt{\frac{(Z_1 - Z_3)^2}{4} + \frac{Z_1 + Z_3}{Y_2} + Z_1 Z_3}. \tag{2.96}$$

In an array of unsymmetric unit cells with $Z_1 \neq Z_3$, the Bloch impedance experienced by the propagating wave depends on its direction. Hence, the two solutions of the Bloch impedance correspond to the wave propagating in positive or negative direction of the periodic structure.

Furthermore, (2.94) and (2.95) yield the dispersion relation

$$e^{j2k^{(\mathrm{T})}p} - (2 + Z_1 Y_2 + Y_2 Z_3) e^{jk^{(\mathrm{T})}p} + 1 = 0 \tag{2.97}$$

so that

$$k^{(\mathrm{T})} = \pm \frac{1}{p} \left[\cos^{-1} \left(1 + \frac{(Z_1 + Z_3) Y_2}{2} \right) + 2m\pi \right]. \tag{2.98}$$

To obtain the same Bloch parameters for the forward and backward propagating wave, the unit cell has to be symmetric with $Z_1 = Z_3 = Z_{\mathrm{se}}/2$ and $Y_2 = Y_{\mathrm{sh}}$ so that (2.96) and (2.98) become

$$Z_{B\mathrm{sym}}^{(\mathrm{T})} = \pm \sqrt{\frac{4Z_{\mathrm{se}} + Z_{\mathrm{se}}^2 Y_{\mathrm{sh}}}{4Y_{\mathrm{sh}}}}, \tag{2.99}$$

$$k^{(\mathrm{T})} = \pm \frac{1}{p} \left[\cos^{-1} \left(1 + \frac{Z_{\mathrm{se}} Y_{\mathrm{sh}}}{2} \right) + 2m\pi \right]. \tag{2.100}$$

Using (2.85) and (2.86), the effective material parameters of the symmetric T-unit cell become

$$\mu_{\mathrm{eff}}^{(\mathrm{T})}(\omega) = \pm \frac{1}{\omega p} \cos^{-1} \left(1 - \frac{(\omega p)^2}{2} \tilde{\mu}\tilde{\varepsilon} \right) \sqrt{\frac{\tilde{\mu}}{\tilde{\varepsilon}} - \left(\frac{\omega p \tilde{\mu}}{2} \right)^2} \tag{2.101}$$

$$\varepsilon_{\mathrm{eff}}^{(\mathrm{T})}(\omega) = \pm \frac{1}{\omega p} \cos^{-1} \left(1 - \frac{(\omega p)^2}{2} \tilde{\mu}\tilde{\varepsilon} \right) \sqrt{\frac{\tilde{\mu}}{\tilde{\varepsilon}} - \left(\frac{\omega p \tilde{\mu}}{2} \right)^2}^{-1} \tag{2.102}$$

where $\tilde{\mu}$ and $\tilde{\varepsilon}$ denote the effective material parameters (2.14) and (2.15) of the distributed structure with $p \to 0$. It can be seen that for a finite unit cell length with $p > 0$, the effective material parameters are not only determined by the unit cell element values, but also by the unit cell length p and the wavenumber of the distributed structure

$$\tilde{k}(\omega) = \omega \sqrt{\tilde{\mu}(\omega)\tilde{\varepsilon}(\omega)}. \tag{2.103}$$

Furthermore, the effective material parameters are not independent of each other since both, the effective permeability and permittivity, are a function of both distributed material parameters and hence, of the series and shunt branch of the unit cell.

For a small unit cell length with $\omega p \ll \frac{1}{\sqrt{\tilde{\mu}(\omega)\tilde{\varepsilon}(\omega)}}$, the inverse cosine becomes

$$\lim_{\omega p \to 0} \frac{1}{\omega p} \cos^{-1}\left(1 - \frac{(\omega p)^2}{2} a\right) = \pm\sqrt{a} \tag{2.104}$$

so that for a small unit cell length compared to guided wavelength, the material parameters of the discrete periodic structure can be approximated by the effective material parameters of the distributed structure:

$$\lim_{\omega p \to 0} \mu_{\text{eff}}^{(\text{T})} = \tilde{\mu}, \tag{2.105}$$

$$\lim_{\omega p \to 0} \varepsilon_{\text{eff}}^{(\text{T})} = \tilde{\varepsilon}. \tag{2.106}$$

For large values of $|\tilde{\mu}(\omega) \cdot \tilde{\varepsilon}(\omega)|$, e.g. close to a Lorentz resonance or for low frequencies in a Drude material, this approximation is not valid and the deviation between the effective material parameters of the discrete and distributed structure becomes significant [22, 23].

Unit Cell in Π-Configuration

Equivalent to the T-configuration, the voltages and currents at the ports of an unsymmetric unit cell in Π-configuration as shown in Fig. 2.13 are

$$V[np] = V[(n+1)p](1 + Z_2 Y_3) + I[(n+1)p] Z_2, \tag{2.107}$$

$$I[np] = V[(n+1)p](Y_1 + Y_1 Z_2 Y_3 + Y_3) + I[(n+1)p](1 + Y_1 Z_2). \tag{2.108}$$

The periodic boundary condition gives

$$V[np] = V[np](1 + Z_2 Y_3) e^{-jk^{(\Pi)}p} + I[np] Z_2 e^{-jk^{(\Pi)}p} \tag{2.109}$$

$$I[np] = V[np](Y_1 + Y_1 Z_2 Y_3 + Y_3) e^{-jk^{(\Pi)}p} + I[np](1 + Y_1 Z_2) e^{-jk^{(\Pi)}p} \tag{2.110}$$

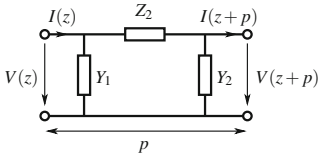


Fig. 2.13 Unit cell in Π-configuration

and with (2.93)

$$Z_B^{(\Pi)} = \frac{Z_2}{e^{jk^{(\Pi)}p} - (1 + Z_2 Y_3)} \tag{2.111}$$

and

$$Z_B^{(\Pi)} = \frac{e^{jk^{(\Pi)}p} - (1 + Y_1 Z_2)}{Y_1 + Y_1 Z_2 Y_3 + Y_3}. \tag{2.112}$$

This yields the Bloch impedance of the unit cell in Π-configuration

$$Z_B^{(\Pi)} = \frac{Z_2(Y_3 - Y_1)}{2(Y_1 + Y_1 Z_2 Y_3 + Y_3)} \pm \sqrt{\left(\frac{Z_2(Y_3 - Y_1)}{2(Y_1 + Y_1 Z_2 Y_3 + Y_3)}\right)^2 + \frac{Z_2}{Y_1 + Y_1 Z_2 Y_3 + Y_3}}. \tag{2.113}$$

The phase terms give the dispersion relation

$$e^{j2k^{(\Pi)}p} - (2 + Y_1 Z_2 + Z_2 Y_3) e^{jk^{(\Pi)}p} + 1 = 0 \tag{2.114}$$

and thus

$$k^{(\Pi)} = \pm \frac{1}{p} \left[\cos^{-1}\left(1 + \frac{(Y_1 + Y_3) Z_2}{2}\right) + 2m\pi \right]. \tag{2.115}$$

As before for the T-configuration, a symmetric unit cell results in a Bloch impedance which is independent of the propagation direction so that with $Y_1 = Y_3 = Y_{\mathrm{sh}}/2$ and $Z_2 = Z_{\mathrm{se}}$ the Bloch impedance is

$$Z_{B\mathrm{sym}}^{(\Pi)} = \pm \sqrt{\frac{4 Z_{\mathrm{se}}}{4 Y_{\mathrm{sh}} + Z_{\mathrm{se}} Y_{\mathrm{sh}}^2}} \tag{2.116}$$

and the wavenumber is

$$k^{(\Pi)} = \pm \frac{1}{p} \left[\cos^{-1}\left(1 + \frac{Z_{\mathrm{se}} Y_{\mathrm{sh}}}{2}\right) + 2m\pi \right] = k^{(\mathrm{T})}. \tag{2.117}$$

With (2.85) and (2.86), the effective material parameters of the symmetric Π-unit cell become

$$\mu_{\mathrm{eff}}^{(\Pi)}(\omega) = \pm \frac{1}{\omega p} \cos^{-1}\left(1 - \frac{(\omega p)^2}{2} \tilde{\mu}\tilde{\varepsilon}\right) \sqrt{\frac{\tilde{\varepsilon}}{\tilde{\mu}} - \left(\frac{\omega p \tilde{\varepsilon}}{2}\right)^2}^{-1} \tag{2.118}$$

$$\varepsilon_{\mathrm{eff}}^{(\Pi)}(\omega) = \pm \frac{1}{\omega p} \cos^{-1}\left(1 - \frac{(\omega p)^2}{2} \tilde{\mu}\tilde{\varepsilon}\right) \sqrt{\frac{\tilde{\varepsilon}}{\tilde{\mu}} - \left(\frac{\omega p \tilde{\varepsilon}}{2}\right)^2} \tag{2.119}$$

which for a small guided wavelength become

$$\lim_{\omega p \to 0} \mu_{\text{eff}}^{(\Pi)} = \tilde{\mu}, \tag{2.120}$$

$$\lim_{\omega p \to 0} \varepsilon_{\text{eff}}^{(\Pi)} = \tilde{\varepsilon}. \tag{2.121}$$

Unit Cell in L-Configuration

The strongly unsymmetric unit cell in L-configuration is a special case of the T- and Π-configuration and can be derived from the T-configuration with the impedance Z_3 set to zero or from the Π-configuration with the admittance Y_1 set to zero. With $Z_1 = Z_2 = Z_{\text{se}}$, $Y_2 = Y_{\text{sh}}$ and $Y_1 = Z_3 = 0$ this yields

$$Z_B^{(\text{L})} = \frac{Z_{\text{se}}}{2} \pm \sqrt{\frac{Z_{\text{se}}^2}{4} + \frac{Z_{\text{se}}}{Y_{\text{sh}}}} \tag{2.122}$$

and

$$k^{(\text{L})} = \pm \frac{1}{p} \left[\cos^{-1}\left(1 + \frac{Z_{\text{se}} Y_{\text{sh}}}{2}\right) + 2m\pi \right]. \tag{2.123}$$

The effective material parameters after the discretization become

$$\mu_{\text{eff}}^{(\text{L})}(\omega) = \frac{1}{\omega p} \cos^{-1}\left(1 - \frac{(\omega p)^2}{2} \tilde{\mu}\tilde{\varepsilon}\right) \left(\frac{j\omega p \tilde{\mu}}{2} \pm \sqrt{\frac{\tilde{\mu}}{\tilde{\varepsilon}} - \left(\frac{\omega p \tilde{\mu}}{2}\right)^2} \right), \tag{2.124}$$

$$\varepsilon_{\text{eff}}^{(\text{L})}(\omega) = \frac{1}{\omega p} \cos^{-1}\left(1 - \frac{(\omega p)^2}{2} \tilde{\mu}\tilde{\varepsilon}\right) \left(\frac{j\omega p \tilde{\mu}}{2} \pm \sqrt{\frac{\tilde{\mu}}{\tilde{\varepsilon}} - \left(\frac{\omega p \tilde{\mu}}{2}\right)^2} \right)^{-1}. \tag{2.125}$$

It can be seen that, due to the unsymmetry of the unit cell, not only the Bloch impedance, but also the effective material parameters depend on the propagation direction, i.e. although a wave experiences the same phase shift for the forward and backward direction, the Bloch impedance and hence, the effective material parameters are different.

As for the T- and Π-configuration, the small wavelength approximation of the effective material parameters becomes

$$\lim_{\omega p \to 0} \mu_{\text{eff}}^{(L)} = \tilde{\mu}, \tag{2.126}$$

$$\lim_{\omega p \to 0} \varepsilon_{\text{eff}}^{(L)} = \tilde{\varepsilon}. \tag{2.127}$$

Discretization of a Lorentz–Drude Material

The impact of discretization on the dispersion parameters and the resulting spatial dispersion is demonstrated for an effective Lorentz–Drude material and a unit cell in T-, Π- and L-configuration. The Lorentz parameters for the effective permeability are $\omega_{0\mu} = 2\pi \cdot 1.1\,\text{GHz}$, $\omega_{\text{t}\mu} = 2\pi \cdot 1.5\,\text{GHz}$, $\delta_\mu = 100\,\text{MHz}$, $\mu_\infty = \mu_0$ and the Drude parameters for the effective permittivity are $\omega_{\text{p}\varepsilon} = 2\pi \cdot 2\,\text{GHz}$, $\delta_\varepsilon = 100\,\text{MHz}$, $\varepsilon_\infty = 2\varepsilon_0$.

In the ideal case for an infinitesimal short unit cell, these parameters yield different propagation and stop bands. Below $\omega_{0\mu}$ the effective permeability and permittivity have different signs which results in a stop band due to the imaginary wavenumber (2.8). The same stop band behavior can be observed between $\omega_{\text{t}\mu}$ and $\omega_{\text{p}\varepsilon}$. In the frequency band between $\omega_{0\mu}$ and $\omega_{\text{t}\mu}$, both, μ'_{eff} and $\varepsilon'_{\text{eff}}$ simultaneously become negative yielding a backward wave band with a negative phase velocity $v_p < 0$. Above $\omega_{\text{p}\varepsilon}$, μ'_{eff} and $\varepsilon'_{\text{eff}}$ are positive resulting in a forward wave band with $v_p > 0$.

The dispersion parameters for the distributed unit cell with $p \to 0$ and for a unit cell length of 10 and 40 mm can be seen in Fig. 2.14 for the T-configuration and in Fig. 2.15 for the Π-configuration, respectively. Using the distributed model, the dispersion parameters are independent of the unit cell configuration. The effective permeability follows the Lorentz dispersion (2.17) whereas the permittivity follows the Drude dispersion (2.24). In the region of simultaneously negative μ'_{eff} and $\varepsilon'_{\text{eff}}$, the wavenumber k becomes negative, while for positive μ'_{eff} and $\varepsilon'_{\text{eff}}$, the wavenumber is positive.

The dispersion properties of the T- and Π-configuration differ when the unit cell length becomes larger. This becomes noticeable near the magnetic resonance frequency of 1.1 GHz, where the wavenumber (2.103) is large. Here, an anti-resonance or resonance occurs in the real part of the effective permittivity [23]. Furthermore, it can be seen that the shape of the effective permeability differs from its original form (2.17).

It can be seen in the plot of the unit cell phase shift that it is saturated at $kp = \pm\pi$, which is the maximum possible unit cell phase shift of a discrete Lorentz–Drude unit cell. Although in the distributed case, the phase shift becomes very large near the magnetic resonance frequency, it is bounded by the discretization and the maximum unit cell phase shift. Hence, the usable bandwidth of the backward wave transmission band becomes smaller with an increased unit cell length.

In Fig. 2.16, the real part of the Bloch impedance and the effective material parameters according to the two solutions of (2.122) of the unit cell in L-configuration are shown. For an infinitesimal short unit cell, both solutions, representing the forward and backward propagating wave, are identical. However, if the unit cell length is increased, the effect of spatial dispersion becomes apparent. As in the T- and Π-configuration, the shape of the effective material parameters differ from the ideal Lorentz–Drude dispersion and resonances occur in the effective permittivity. Furthermore, all dispersion parameters except the phase are different for waves in forward and backward direction.

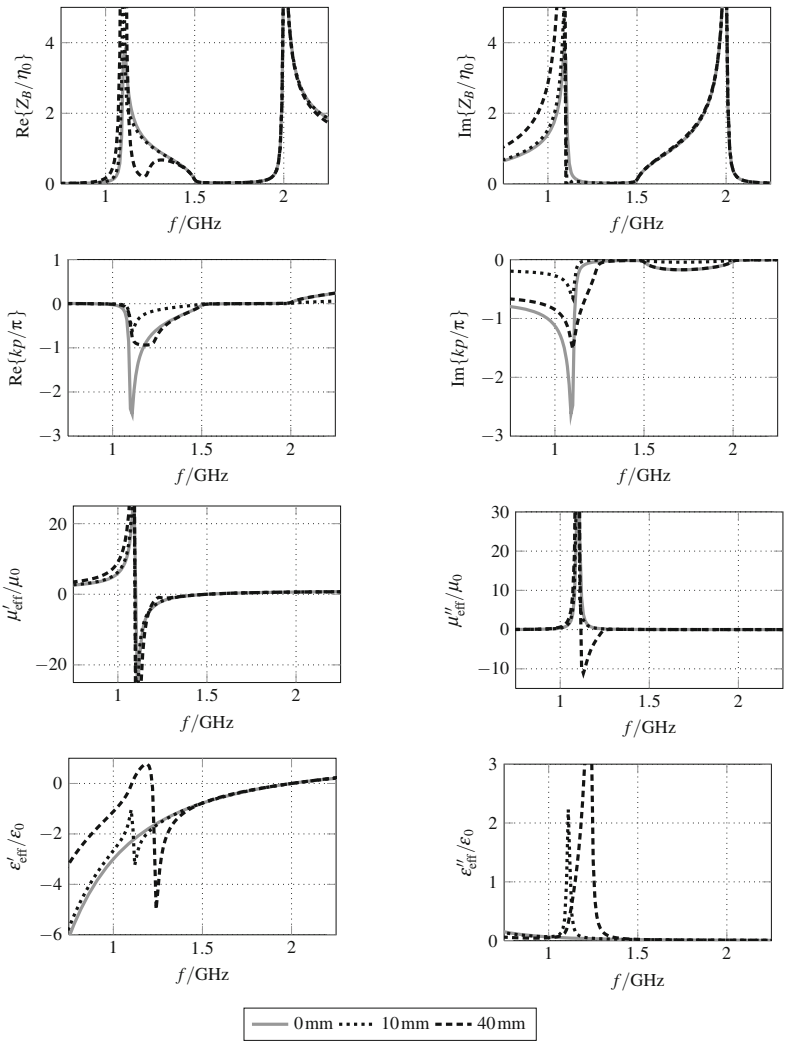


Fig. 2.14 Impact of the unit cell length on the dispersion parameters of a symmetric unit cell in T-configuration

Due to the equivalence between effective material parameters and transmission line parameters (2.85) and (2.86), the impact of discretization depends on the unit cell circuit and not on the geometry of the unit cell. Hence, the presented considerations are valid for one-dimensional artificial transmission lines as well as for two- and three-dimensional lattices.

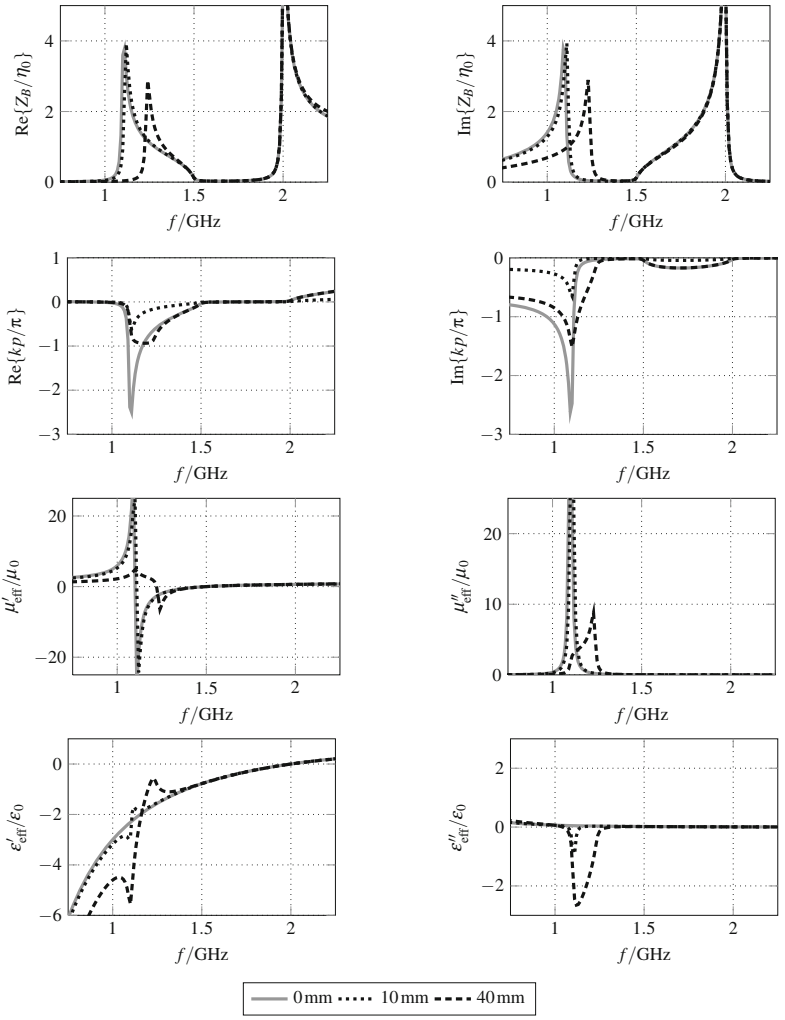


Fig. 2.15 Impact of the unit cell length on the dispersion parameters of a symmetric unit cell in Π-configuration

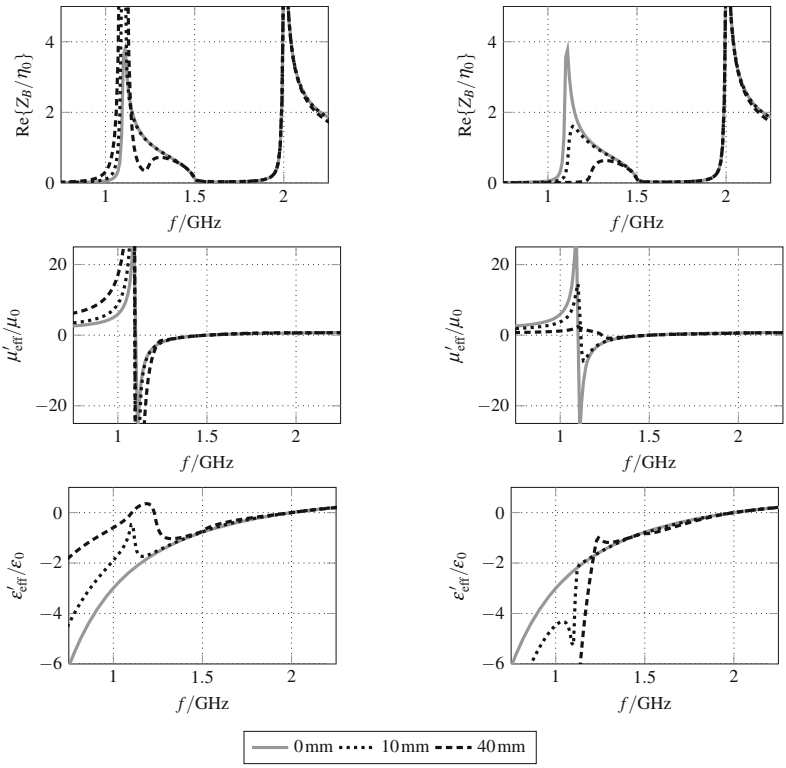


Fig. 2.16 Impact of the unit cell length on the real part of the Bloch impedance and the effective material parameters of a unit cell in unsymmetric L-configuration

References

1. J.D. Jackson, *Classical Electrodynamics*, 3rd edn. (Wiley, New York, 1998)
2. D. Pozar, *Microwave Engineering* (Wiley, New York, 2012)
3. G. Eleftheriades, A. Iyer, P. Kremer, Planar negative refractive index media using periodically L-C loaded transmission lines. IEEE Trans. Microw. Theory Tech. **50**, 2702–2712 (2002)
4. K .G. Eleftheriades, G.V. Balmain, *Negative-Refraction Metamaterials—Fundamental Principles and Applications* (Wiley, New York, 2005)
5. A.D. Rakić, A.B. Djurišić, J.M. Elazar, M.L. Majewski, Optical properties of metallic films for vertical-cavity optoelectronic devices. Appl. Opt. **37**, 5271–5283 (1998)
6. H.M. Nussenzveig, *Causality and Dispersion Relations* (Academic Press, New York, 1972)
7. T.M. Grzegorczyk, M. Nikku, X. Chen, B.-I. Wu, J.A. Kong, Refraction laws for anisotropic media and their application to left-handed metamaterials. IEEE Trans. Microw. Theory Tech. **53**(4), 1443–1450 (2005)
8. V.G. Veselago, The electrodynamics of substances with simultaneously negative values of ϵ and μ. Sov. Phys. Uspekhi **10**(4), 509 (1968)
9. L.D. Landau, E.M. Lifshitz, A.L. King, Electrodynamics of continuous media. Am. J. Phys. **29**(9), 647–648 (1961)

10. B. Girod, R. Rabenstein, A. Stenger, Einführung in die Systemtheorie: Signale und Systeme in der Elektrotechnik und Informationstechnik. Lehrbuch Elektrotechnik (Vieweg+Teubner Verlag, 2007)
11. J.S. Toll, Causality and the dispersion relation: logical foundations. Phys. Rev. **104**, 1760–1770 (1956)
12. R.L. Weaver, Y.-H. Pao, Dispersion relations for linear wave propagation in homogeneous and inhomogeneous media. J. Math. Phys. **22**(9), 1909–1918 (1981)
13. R. Bracewell, *The Fourier Transform and Its Applications*, McGraw-Hill Series in Electrical and Computer Engineering (McGraw Hill, New York, 2000)
14. A. Iyer, G. Eleftheriades, Negative refractive index metamaterials supporting 2-d waves, in *2002 IEEE MTT-S International Microwave Symposium Digest*, vol. 2 (2002), pp. 1067–1070
15. A. Lai, T. Itoh, C. Caloz, Composite right/left-handed transmission line metamaterials. IEEE Microw. **5**(3), 34–50 (2004)
16. C. Caloz, Dual composite right/left-handed (D-CRLH) transmission line metamaterial. IEEE Microw. Wirel. Compon. Lett. **16**, 585–587 (2006)
17. R.M. Foster, A reactance theorem. Bell Syst. Tech. J. **3**(2), 259–267 (1924)
18. M.I. Stockman, Criterion for negative refraction with low optical losses from a fundamental principle of causality. Phys. Rev. Lett. **98**, 177404+ (2007)
19. V.V. Varadan, R. Ro, Unique retrieval of complex permittivity and permeability of dispersive materials from reflection and transmitted fields by enforcing causality. IEEE Trans. Microw. Theory Tech. **55**, 2224–2230 (2007)
20. Z. Szabo, G.-H. Park, R. Hedge, E.-P. Li, A unique extraction of metamaterial parameters based on Kramers–Kronig relationship. IEEE Trans. Microw. Theory Tech. **58**(10), 2646–2653 (2010)
21. R. Collin, I. Antennas, P. Society, Field theory of guided waves, in *The IEEE/OUP Series on Electromagnetic Wave Theory (Formerly IEEE Only)*. Series Editor Series (IEEE Press, 1991)
22. C.R. Simovski, S.A. Tretyakov, Local constitutive parameters of metamaterials from an effective-medium perspective. Phys. Rev. B **75**, 195111 (2007)
23. T. Cui, D. Smith, R. Liu, *Metamaterials: Theory, Design, and Applications* (Springer, New York, 2009)

http://www.springer.com/978-3-319-28178-0

Tunable Microwave Metamaterial Structures

Maasch, M.

2016, XVII, 138 p. 143 illus., 122 illus. in color.,
Hardcover
ISBN: 978-3-319-28178-0